Journal of Biomolecular NMR, 9 (1997) 397–407

J-Bio NMR 431

Hydrogen–deuterium exchange studies of the rat thyroid transcription factor 1 homeodomain

Gennaro Esposito*, Federico Fogolari, Giuseppe Damante, Silvestro Formisano**, Gianluca Tell, Antonio Leonardi, Roberto Di Lauro*** and Paolo Viglino

Dipartimento di Scienze e Tecnologie Biomediche, Università degli Studi di Udine, Via Gervasutta 48, I-33100 Udine, Italy

Received 22 November 1996
Accepted 27 January 1997

Keywords: Thyroid transcription factor 1 homeodomain; Homeodomain; DNA-binding proteins; Protein NMR; Hydrogen–deuterium exchange; Secondary structure thermal stability

Summary

The ^{1}H NMR solution structure of the rat thyroid transcription factor 1 homeodomain (TTF-1 HD) showed that the molecule folds like classical homeodomains. The C-terminal extension of helix III (fragment 51–59) appeared to adopt a helical geometry, albeit not as rigid as the preceding portion, but the hydrogen–deuterium exchange of backbone amides and the NOE data provided evidence of a discontinuity between the two moieties of helix III at the highly conserved fragment Asn^{51}–His^{52}–Arg^{53}. Analysis of quantitative measurements of isotope exchange rates allows one to recognize the general occurrence, in that region of HD motifs, of opposite effects to helix III stability. Asparagine, histidine and arginine residues occur most frequently at the beginning and end of protein helices. In TTF-1 HD a local fluctuation is observed in the fragment 51–53 which either kinks or tightens the α-helix. A search through the protein structure database reveals that the three most common variants of HD fragments 51–53 are often involved in helices and, frequently, in helix initiation or termination. For homeodomains in general, the nature of the fragment 51–53 may be related to the conformational dynamics of their DNA-recognition helix (helix III). Besides the specific results on fragment 51–53, the complete isotope exchange analysis of TTF-1 HD data shows that the partially solvent-exposed recognition helix is stabilized by hydrophobic interactions, like most of the structured regions of the molecule. Hydrophobic stabilization of the contacting regions meets the requirements of a DNA-interaction mechanism which, as shown with other DNA-protein complexes, should entail negative heat capacity variations due to changes in solvent exposure of the nonpolar protein surface.

Introduction

Homeodomains are a very well-known class of DNA-binding domains occurring in a large family of transcriptional activators involved in the determination of cell development and the specification of body plan (Gehring, 1987; Pabo and Sauer, 1992; Gehring et al., 1994b). A number of structural studies by X-ray diffractometry (Kissinger et al., 1990; Wolberger et al., 1991; Ceska et al., 1993; Klemm et al., 1994) and NMR spectroscopy (Otting et al., 1988,1990; Qian et al., 1989,1993,1994; Billeter et al., 1990,1993; Phillips et al., 1991; Leiting et al., 1993; Morita et al., 1993; Viglino et al., 1993; Sivaraja et al., 1994; Tsao et al., 1994; Cox et al., 1995) have shown that homeodomains share a common folding pattern.

The tertiary structure of the homeodomain (HD) of the rat thyroid transcription factor 1 (TTF-1), a 378-residue protein responsible for transcriptional activation of genes

*To whom correspondence should be addressed.
**Present address: Dipartimento di Biologia e Patologia Cellulare e Molecolare, Università di Napoli 'Federico II', Via Pansini 5, I-80134 Napoli, Italy.
***Present address: Stazione Zoologica 'A. Dohrn', Villa Comunale 1, I-80123 Napoli, Italy.

Abbreviations: TTF-1, thyroid transcription factor 1; *Antp*, *Antennapedia*; *ftz*, *fushi tarazu*; LFB1/HNF1, liver factor binding 1/hepatocyte nuclei factor 1; BPTI, bovine pancreatic trypsin inhibitor; HD, homeodomain; H-D, hydrogen–deuterium; HTH, helix-turn-helix; 2D, two-dimensional; NOE, nuclear Overhauser enhancement; NOESY, nuclear Overhauser enhancement spectroscopy; TOCSY, total correlation spectroscopy.

TABLE 1
HYDROGEN–DEUTERIUM EXCHANGE DATA OF TTF-1 HD BACKBONE AMIDES[a]

T (K)/pH*	284.0/4.02		278.7/4.13		273.4/4.02		ΔH (kcal/mol) 284.0–273.4 K
	log k_{app}	log K_1	log k_{app}	log K_1	log k_{app}	log K_1	
Met^{0}							
Arg^{1}	> –2		> –2		> –2		
Arg^{2}	> –2		> –2		> –2		
Lys^{3}	> –2		> –2		> –2		
Arg^{4}	> –2		> –2		> –2		
Arg^{5}	> –2		> –2		> –2		
Val^{6}	> –2		> –2		> –2		
Leu^{7}	> –2		> –2		> –2		
Phe^{8}	> –2		> –2		> –2		
Ser^{9}	–2.486 ± 0.023	0.043 ± 0.023	–2.686 ± 0.032	0.218 ± 0.032	–3.696 ± 0.093	–0.199 ± 0.093	+8.3 ± 2.3
Gln^{10}	> –2		> –2		> –2		
Ala^{11}	> –2		> –2		> –2		
Gln^{12}	–3.579 ± 0.055	–0.645 ± 0.055	–3.875 ± 0.162	–0.573 ± 0.162	–3.597 ± 0.064	0.257 ± 0.064	–13.1 ± 0.9
Val^{13}	–3.713 ± 0.121	–0.779 ± 0.121	–4.331 ± 0.372	–1.029 ± 0.372	< –4.398 –0.434	< –0.544 –0.434	> –8.03 (*10.6*)
Tyr^{14}	< –4.398 –0.434	< –1.262 –0.434	–	–	< –4.398 –0.434	< –0.383 –0.434	> –29.5 u.e.
Glu^{15}	–4.208 ± 0.146	–1.359 ± 0.146	–3.800 ± 0.117	–0.582 ± 0.117	< –4.398 –0.434	< –0.614 –0.434	> –24.7 (*9.4*)
Leu^{16}	< –4.398 –0.434	< –1.463 –0.434	–4.318 ± 0.361	–1.015 ± 0.361	< –4.398 –0.434	< –0.544 –0.434	> –30.8 u.e.
Glu^{17}	–3.471 ± 0.068	–0.536 ± 0.068	–3.573 ± 0.157	–0.271 ± 0.157	–3.538 ± 0.172	0.316 ± 0.172	–28.6 ± 3.5
Arg^{18}	–3.881 ± 0.156	–1.032 ± 0.156	–4.196 ± 0.272	–0.979 ± 0.272	–3.412 ± 0.075	0.374 ± 0.075	–47.4 ± 2.5
Arg^{19}	–4.015 ± 0.116	–1.300 ± 0.116	–3.841 ± 0.182	–0.753 ± 0.182	–4.135 ± 0.199	–0.467 ± 0.199	–27.9 ± 2.8
Phe^{20}	–3.217 ± 0.280	–0.324 ± 0.280	–	–	–	–	–
Lys^{21}	–3.303 ± 0.045	–0.410 ± 0.045	–3.545 ± 0.172	–0.283 ± 0.172	–3.919 ± 0.178	–0.095 ± 0.178	–10.6 ± 4.6
Gln^{22}	–2.724 ± 0.005	–0.054 ± 0.005	–3.010 ± 0.012	0.031 ± 0.012	–4.093 ± 0.126	–0.467 ± 0.126	+14 ± 4
Gln^{23}	–2.103 ± 0.010	0.702 ± 0.010	–2.363 ± 0.017	0.812 ± 0.017	–3.596 ± 0.034	0.149 ± 0.034	+22.4 ± 0.8
Lys^{24}	–2.140 ± 0.029	0.621 ± 0.029	–2.498 ± 0.043	0.634 ± 0.043	–2.965 ± 0.035	0.743 ± 0.035	–4.11 ± 0.22
Tyr^{25}	–2.254 ± 0.092	0.638 ± 0.092	–2.214 ± 0.099	1.048 ± 0.099	–2.692 ± 0.020	1.130 ± 0.020	–16.4 ± 2.4
Leu^{26}	> –2		> –2		> –2		
Ser^{27}	–2.382 ± 0.017	0.241 ± 0.017	–2.700 ± 0.025	0.295 ± 0.025	–3.696 ± 0.064	–0.114 ± 0.064	+12.0 ± 1.6
Ala^{28}	> –2		> –2		> –2		
Pro^{29}							
Glu^{30}	–3.046 ± 0.023	–0.111 ± 0.023	–3.544 ± 0.099	–0.242 ± 0.099	< –4.398 –0.434	< –0.544 –0.434	> +14.5 (*14*)
Arg^{31}	–3.673 ± 0.127	–0.377 ± 0.127	< –4.398 –0.434	< –1.179 –0.434	< –4.398 –0.434	< –0.613 –0.434	> +7.60 u.e.
Glu^{32}	–3.499 ± 0.104	–0.830 ± 0.104	–3.714 ± 0.256	–0.674 ± 0.256	–	–	–
His^{33}	–2.492 ± 0.261	–0.888 ± 0.261	–2.139 ± 0.722	–0.159 ± 0.722	–3.533 ± 0.276	–0.935 ± 0.276	+1.90 ± 2.16
Leu^{34}	–3.227 ± 0.035	–1.228 ± 0.035	–	–	–	–	–
Ala^{35}	–3.293 ± 0.219	–0.237 ± 0.219	–3.525 ± 0.691	–0.105 ± 0.691	–	–	–
Ser^{36}	–3.311 ± 0.037	–0.687 ± 0.037	–3.518 ± 0.120	–0.524 ± 0.120	–4.068 ± 0.164	–0.485 ± 0.164	–6.7 ± 4.3
Met^{37}	–3.456 ± 0.033	–0.651 ± 0.033	–3.513 ± 0.067	–0.307 ± 0.067	< –4.398 –0.434	< –0.652 –0.434	> +0.180 (*13*)
Ile^{38}	< –4.398 –0.434	< –1.342 –0.434	< –4.398 –0.434	< –0.979 –0.434	< –4.398 –0.434	< –0.450 –0.434	< –29.9 u.e.
His^{39}	–2.118 ± 0.025	–0.367 ± 0.025	–2.451 ± 0.044	–0.322 ± 0.044	–3.466 ± 0.070	–0.721 ± 0.070	+12.0 ± 1.5
Leu^{40}	–3.645 ± 0.029	–1.646 ± 0.029	–3.676 ± 0.036	–1.302 ± 0.036	< –4.398 –0.434	< –1.410 –0.434	> –7.81 (*13*)
Thr^{41}	–3.944 ± 0.133	–1.321 ± 0.133	–3.963 ± 0.127	–0.968 ± 0.127	< –4.398 –0.434	< –0.815 –0.434	> –16.9 (*10.3*)
Pro^{42}							
Thr^{43}	> –2		> –2		> –2		
Gln^{44}	–3.391 ± 0.062	–0.721 ± 0.062	–3.500 ± 0.072	–0.458 ± 0.072	–4.106 ± 0.196	–0.480 ± 0.196	–8.0 ± 4.4
Val^{45}	–4.265 ± 0.320	–1.332 ± 0.320	–3.822 ± 0.175	–0.521 ± 0.175	–3.790 ± 0.121	0.064 ± 0.121	–46.7 ± 6.7
Lys^{46}	< –4.398 –0.434	< –1.420 –0.434	< –4.398 –0.434	< –1.056 –0.434	–3.703 ± 0.080	0.190 ± 0.080	< –54.1 u.e.
Ile^{47}	–4.187 ± 0.279	–1.382 ± 0.279	< –4.398 –0.434	< –1.123 –0.434	–3.432 ± 0.327	0.313 ± 0.327	< –57.0 (*1.8*)
Trp^{48}	< –4.398 –0.434	< –2.699 –0.434	< –4.398 –0.434	< –2.301 –0.434	–3.771 ± 0.177	–1.027 ± 0.177	< –56.2 u.e.
Phe^{49}	< –4.398 –0.434	< –2.301 –0.434	< –4.398 –0.434	< –1.921 –0.434	–	–	–
Gln^{50}	–3.990 ± 0.194	–1.143 ± 0.194	–3.560 ± 0.152	–0.341 ± 0.152	–3.246 ± 0.073	0.539 ± 0.073	–56.4 ± 4.0
Asn^{51}	–2.771 ± 0.023	–0.194 ± 0.023	–3.260 ± 0.207	–0.311 ± 0.207	< –4.398 –0.434	< –0.854 –0.434	> +22.2 (*14*)
His^{52}	–2.370 ± 0.078	–1.066 ± 0.078	–2.201 ± 0.102	–0.519 ± 0.102	< –4.398 –0.434	< –2.097 –0.434	> +35.0 (*12*)
Arg^{53}	–3.123 ± 0.056	–1.223 ± 0.056	–2.793 ± 0.077	–0.517 ± 0.077	< –4.398 –0.434	< –1.507 –0.434	> +9.88 (*12*)
Tyr^{54}	> –2		> –2		> –2		
Lys^{55}	> –2		> –2		> –2		
Met^{56}	> –2		> –2		> –2		
Lys^{57}	> –2		> –2		> –2		

TABLE 1
(continued)

T (K)/pH*	284.0/4.02		278.7/4.13		273.4/4.02		ΔH (kcal/mol) 284.0–273.4 K
	log k_{app}	log K_l	log k_{app}	log K_l	log k_{app}	log K_l	
Arg[58]	−3.317 ± 0.121	−0.602 ± 0.121	−2.881 ± 0.058	0.206 ± 0.058	−3.122 ± 0.020	0.546 ± 0.020	−38.4 ± 3.4
Gln[59]	> −2		> −2		> −2		
Ala[60]	> −2		> −2		> −2		
Lys[61]	> −2		> −2		> −2		
Asp[62]	> −2		> −2		> −2		
Lys[63]	> −2		> −2		> −2		
Ala[64]	> −2		> −2		> −2		
Ala[65]	> −2		> −2		> −2		
Gln[66]	> −2		> −2		> −2		
Gln[67]	> −2		> −2		> −2		

[a] The logarithm value of the apparent exchange rate and local destructuring equilibrium constant (k_{app}/min^{-1} and K_l, respectively, Eq. 3) are reported for T = 284.0, 278.7 and 273.4 K, at the indicated pH*. The enthalpy variations, calculated from the linear fit of ln K_l versus 1/T, in the range 284.0–273.4 K, are also given. Only the upper limits of k_{app}, obtained from slowly exchanging amides, were employed for estimating the corresponding K_l upper limits. When more than one available K_l value for an individual NH was an upper limit, a decision on the corresponding ΔH was taken from additional experimental data at T = 273.4 K and pH* = 4.07 (not listed). A dash is reported when the specific NH connectivity was not detectable. The errors are expressed in logarithmic units for k_{app} and K_l, and in kcal/mol for ΔH. Underscored error values indicate the single-sided error band affecting the corresponding upper-limit kinetic or equilibrium constants. Italicized values in parentheses are ΔH error limits and u.e. indicates undetermined ΔH error (see the Materials and Methods section).

expressed only in follicular thyroid cells (Guazzi et al., 1990) and lung epithelial cells (Bohinski et al., 1994), has recently been determined by NMR spectroscopy (Esposito et al., 1996) and deposited in the Brookhaven Protein Databank (code 1FTT). Like all other family members, TTF-1 HD folds into a three-helix structural domain. Helices I and II, which are connected by a loose loop, run approximately antiparallel, and both are approximately perpendicular to helix III. The latter, referred to as a recognition helix, forms with the tight turn junction to helix II the helix-turn-helix (HTH) motif, occurring also in prokaryotic repressors, and is expected to contact the major groove of the polynucleotide target (Fogolari et al., 1993). Beyond the analogy with the general HD folding pattern, two additional features emerged from the NMR characterization of TTF-1 HD, concerning the helix N-capping motifs and the stability of the recognition helix.

The presence of N-capping motifs at the helices of TTF-1 HD is common to all homeodomains, but has only previously been noticed for *Antennapedia* (*Antp*) HD (Otting et al., 1988). The similarities among homeodomains concerning N-capping of helices extend further, because also the stability of helix I and helix III N-cappings, opposite to the lability of that at helix II, is a general trend amongst homeodomains. Whilst the tendency to helix-capping motifs may be understood because they increase stability and probably assist folding (Presta and Rose, 1988; Richardson and Richardson, 1988; Bell et al., 1992; Zhou et al., 1993), the lability of the helix II N-capping can be related, from HD sequence covariance analysis (Clarke, 1995), to the exclusive predominance of the salt bridge involving residues 19 and 30, the latter being the N3 location (Richardson and Richardson, 1988) of helix II which is required for engaging the local capping interaction.

The structural stability of the recognition helix in isolated homeodomains marks an important difference within this class of molecules, namely between those homeodomains with a largely helical C-terminal extension of the recognition helix and those where this region appears heavily frayed. Typical examples of the two subclasses are *Antp* (Billeter et al., 1990) and *fushi tarazu* (*ftz*) HD (Qian et al., 1994), respectively. In spite of the increase in local mobility, the C-terminal region of TTF-1 HD recognition helix is still helically ordered, at variance with the highly homologous (82%) NK-2 HD (Tsao et al., 1994). In this respect, TTF-1 HD is similar to the more distant *Antp* HD. The NOE data for TTF-1 HD are consistent with either a kinking or tightening in the fluctuation of the α-helix at the fragment 51–53 (Esposito et al., 1996). Neither the kink nor the tightening were reproduced in the restrained final structures, however. In view of the involvement of the fragment 50–54 in HD-DNA recognition and of the unique DNA-binding specificity of TTF-1 HD, which preferentially binds the 5'-CAAG-3' core stretch, rather than 5'-TAAT-3' (Guazzi et al., 1990; Damante et al., 1994a,1996), these results suggest that additional investigations are necessary to elucidate the fine details of the recognition mechanism. We have therefore extended the previous hydrogen–deuterium (H-D) exchange studies of TTF-1 HD (Viglino et al., 1993; Esposito et al., 1996) on a quantitative basis, over a narrow temperature range, below that which was chosen for the structure determination (284–287 K). The aim was to gain further insight into local conformational dynamics through information inferred from isotope exchange rates.

Materials and Methods

Sample preparation and operating conditions

The polypeptide encompassing TTF-1 HD (68 residues corresponding to fragment 160–226 of the entire rat TTF-1 protein, plus a methionyl residue at the N-terminus referred to as Met^0, MW = 8443.9 Da) was obtained as described earlier (Guazzi et al., 1990; Viglino et al., 1993).

For the H-D exchange experiments, the protein was first dissolved in H_2O and heated for 1 h at 323 K after pH adjustment to 4.0–4.2. The sample was then recovered by lyophilization and redissolved in D_2O (99.9%, Sigma) in an ice-water bath, where the solvent, the NMR tube and the protein powder itself had been pre-equilibrated. Measurements were quickly started and the pH* (uncorrected meter reading) was checked only afterwards (its value was always approximately the same as that preset in H_2O). Preliminary additions of NaN_3 to the solvent (0.2–0.5% weight/volume) were always performed to preserve the protein, whose concentration was approximately 5.5 mM.

^{1}H NMR spectra were collected at 500.13 MHz on a Bruker AM500 spectrometer. The actual probe temperature was carefully determined (accuracy ±0.2 K) from resonance separation of methanol.

All 2D spectra were acquired in pure-phase mode using time-proportional phase incrementation for t_1 quadrature (Marion and Wüthrich, 1983). Processing was performed with Felix software (Biosym Technologies, San Diego, CA, U.S.A.). To avoid introduction of a baseline offset in F1, 2D experiments were acquired with appropriate shifting of the first data point (Bax et al., 1991). During processing, linear prediction was applied from this point to back-reconstruct the missing point (Marion and Bax, 1989). Baseline flatness was optimized in the t_2 domain by appropriate setting of the pre-acquisition delay and analog filter level, and by a ninth-order polynomial baseline correction during processing. Prior to processing, data were multiplied by 90°-shifted sine-squared bell window functions and zero-filled in both dimensions to end up with data matrix sizes of 2048×2048 real points.

H-D isotope exchange measurements

The time-course of the NH-αH connectivities was monitored in three series of clean-TOCSY (Griesinger et al., 1988) experiments, which were collected at computer-controlled time intervals within the first 20 h from sample preparation at 273.4, 278.7 and 284.0 K, with pH* = 4.07, 4.13 and 4.02, respectively.

All spectra were acquired with 1024 data points in t_2 and 256 t_1 increments (eight transients plus two dummy scans per increment) over a sweep width of 7042 Hz in both dimensions, and with the same recycling time (1 s) and isotropic mixing (15.8 ms at $\gamma B_2/2\pi = 12.5$ kHz), to ensure a constant sampling time within each series and, as far as possible, throughout all series (59.6 min/experiment). An invariant data processing protocol was also employed (see above) before quantitation of the NH-αH connectivity amplitudes, whose time-course was analysed by means of an exponential fitting routine to evaluate the apparent kinetic constant of the isotope exchange reaction (see below).

H-D exchange is not negligible during the measuring time, but since it takes place at constant conditions during either measuring and waiting intervals we can write (Wagner and Wüthrich, 1982)

$$I(t) = I_0 e^{-kt_{el}} \int_0^{t_{rec}} \frac{e^{-kt}}{t_{rec}}\, dt = I_0 e^{-kt_{el}} \left[\frac{-1}{kt_{rec}} \left(e^{-kt_{rec}} - 1 \right) \right] \quad (1)$$

where k is the kinetic constant, t_{el} is the elapsed time from sample preparation to starting of the experiment, t_{rec} is the experiment recording time, and I_0 and I(t) are the initial and time-dependent amplitudes of the connectivities. Since the right-hand bracketed factor of Eq. 1 is constant because all recordings have the same duration, the experimental amplitudes can be fitted by

$$I(t) = I_0 C e^{-kt_{el}} \quad (2)$$

where

$$C = -\left[\frac{1}{kt_{rec}} \left(e^{-kt_{rec}} - 1 \right) \right]$$

The experimental measurement conditions set limits for the measurable kinetic constants. We estimate an upper limit of 1×10^{-2} min^{-1} and a lower limit of 4×10^{-5} min^{-1}, provided that 5% residual or differential intensity, with respect to the first sampled intensity figure, can be detected for the third point (~240 min of exchange) or the last point (~1200 min of exchange), respectively. The experimental uncertainty in the measured intensities also determines the errors in the apparent exchange constants (Table 1), which in turn affect the values of K_1 and ΔH. Since no error estimation is available for the k_{int} constants (Eq. 3), only a lower-error-limit estimate is possible for each K_1 by imposing $\Delta K_1 = \Delta k_{app}/\text{min}^{-1}$. The Δk_{app} values are the uncertainties affecting the corresponding fitting parameter of the experimental intensity exponential decay. A Δk_{app} ($=\Delta K_1$ min^{-1}) $= -4 \times 10^{-5}$ min^{-1} was assumed when only upper-limit k_{app} values could be measured (corresponding to a −100% error, with a single-sided flat distribution). The listed ΔH errors (Table 1) were computed from the average slope uncertainty of van 't Hoff plots. No meaningful ΔH error estimation could be obtained when two or more upper-limit K_1 constants were involved, whilst an upper-limit value of ΔΔH was computed anyway (and reported in italics in Table 1) when only one, out of three intervening K_1 values, was an upper limit.

Results

Dissecting the isotope exchange process of amide hydrogens

Previously reported hydrogen–deuterium (H-D) isotope exchange data (Viglino et al., 1993) had been obtained from NH-αH cross peaks of two TOCSY spectra that were recorded sequentially, immediately after dissolving the lyophilized protein sample in D_2O at 287 K and pH* = 4.02. Since the measured amplitudes reflected the average exchange that had occurred throughout each experiment (approximately 6 and 11.5 h after dissolving), we could broadly classify the amide hydrogens into classes, depending on the extent of intensity loss (limited or extensive) during the first experiment and on the further loss (minor, substantial or total) after 11.5 h of D_2O exposure. The qualitative picture that was obtained has been confirmed by the quantitative determinations of the amide exchange rates we present here.

Exponential fitting of the time-course of the clean-TOCSY NH-αH cross-peak amplitudes in H-D exchange experiments provides the apparent kinetic constants (k_{app}) for isotope exchange of the individual backbone amide protons. These k_{app} values at 284 K have already been employed to draw the qualitative classification into fast, medium and slow exchanging amides that was presented with the tertiary structure determination (Esposito et al., 1996). The whole set of data obtained from experiments that were performed in the range 273.4–284.0 K is reported in Table 1.

The isotope exchange process undergone by backbone amide hydrogens when a protein is dissolved in D_2O can be summarized by

$$NH_n \underset{k_{cl}}{\overset{k_{op}}{\leftrightarrows}} NH_0 \xrightarrow{k_{int}} ND_0 \underset{k_{op}}{\overset{k_{cl}}{\leftrightarrows}} ND_n$$

where the subscripts n and o denote the native (closed) and open conformations, and k_{op}, k_{cl} and k_{int} denote the kinetic constants for the opening, closing and isotope exchange steps, respectively.

When far from denaturing conditions (i.e. when $k_{op} \ll k_{cl}$), if $k_{cl} \gg k_{int}$, the apparent kinetic constant of the resulting exchange process (EX2) can be written as (Hvidt and Nielsen, 1966)

$$k_{app} \cong \frac{k_{op}}{k_{cl}} \times k_{int} = K_1 \times k_{int} \qquad (3)$$

which allows one to extract the local destructuring equilibrium constant K_1 ($= k_{op}/k_{cl}$) from the experimentally determined k_{app} values (Wagner et al., 1984), once the intrinsic exchange kinetic constants (k_{int}) are evaluated (Molday et al., 1972). The calculation of the reference k_{int} value was performed based on the equation for specific acid, specific base and water catalysis (Englander and Kallenbach, 1984):

$$k_{int} = k_A[D^+] + k_B[OD^-] + k_w \qquad (4)$$

by using the recently redetermined values of the kinetic constants k_A, k_B and k_w (Jeng and Englander, 1991), $[D^+] = 10^{-pH^*}$ and $[OD^-] = 10^{-(pK_{D_2O} - pH^*)}$. Appropriate corrections for each experimental temperature were applied to the specific catalysis constants of Eq. 4 and to pK_{D_2O}, respectively, by using $\Delta E_A^{\ddagger} = 14$ kcal/mol, $\Delta E_B^{\ddagger} = 17.5$ kcal/mol and $\Delta E_w^{\ddagger} = 21$ kcal/mol (1 cal = 4.184 J) (Englander and Kallen-

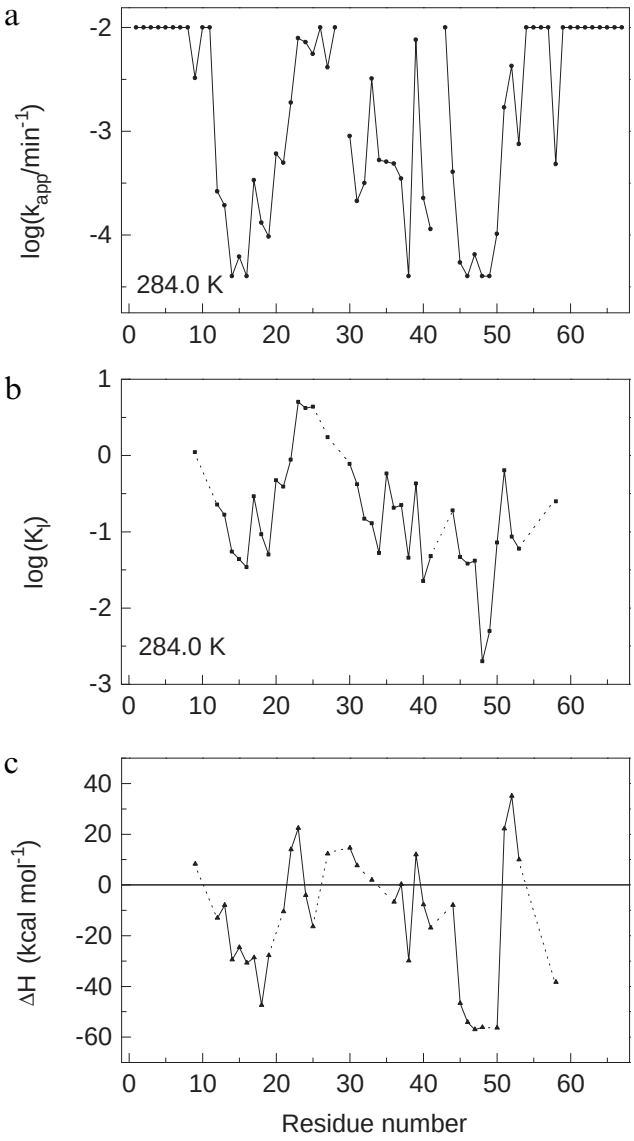

Fig. 1. Kinetic and thermodynamic parameters from isotope exchange analysis of TTF-1 HD backbone amides. The entire data set is listed in Table 1, where explicit indication about the nature of the upper or lower limit of the reported parameters is provided, along with the corresponding errors. (a) Apparent exchange rates (Eq. 3) versus residue number. Interpolation segments are not drawn between residues separated by proline residues. (b) Local destructuring equilibrium constants versus residue number evaluated from data in (a) according to Eq. 3. Broken segments join the calculated values when one or more consecutive points are not available. (c) ΔH of the local destructuring process versus residue number from the linear fit of van 't Hoff curves. As in (b), broken segments are drawn when gaps occur in the available data set.

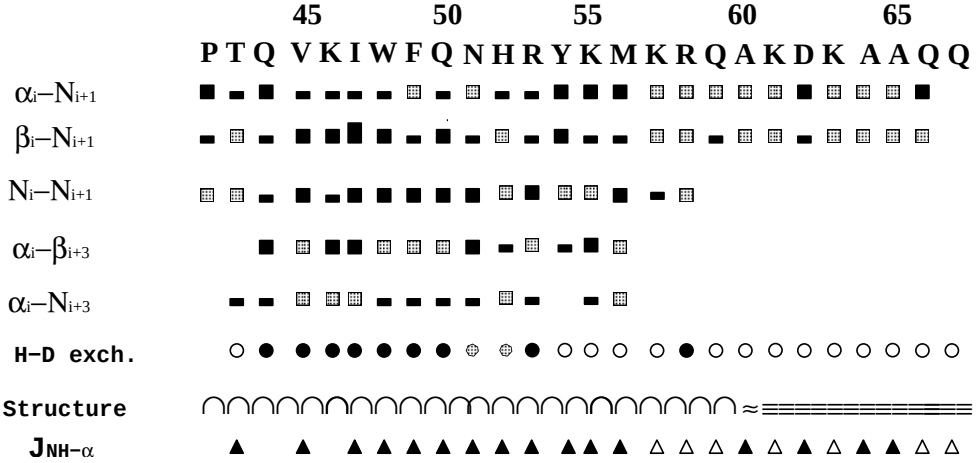

Fig. 2. Summary of the relevant secondary structure diagnostic NOEs observed for the recognition helix of TTF-1 HD. The relative strength of the various types of NOEs is indicated by the size of the filled boxes in correspondence of the amino acid sequence given at the top of the diagram. For this purpose, NOEs were classified as strong (upper distance bound ≤ 3 Å), medium (3 Å < upper distance bound < 3.5 Å) and weak (upper distance bound ≥ 3.5 Å). Shadowed boxes indicate connectivities that could not be safely integrated because of partial overlap. Backbone amide exchange data are reported according to the corresponding apparent exchange rate (k_{app}) measured at 284 K (Table 1), i.e. $k_{app} \leq 1 \times 10^{-3}$ min^{-1}, filled circle; 1×10^{-3} $min^{-1} < k_{app} < 1 \times 10^{-2}$ min^{-1}, shadowed circle; $k_{app} \geq 1 \times 10^{-2}$ min^{-1}, empty circle. $J_{NH-\alpha}$ estimates are provided when available (Esposito et al., 1996). A filled triangle indicates $J_{NH-\alpha} < 6$ Hz, an empty triangle $J_{NH-\alpha} \geq 6$ Hz. The secondary structure symbols correspond to: disordered region (straight lines), fraying edge (weavy lines), α-helix (curly line).

bach, 1984; Jeng and Englander, 1991) in the empirical extension of the van 't Hoff equation, and the relationship (Covington et al., 1966)

$$pK_{D_2O} = 4913T^{-1} - 7.60 + 0.02009T$$

where T is the absolute temperature. The sequence-specific corrections (Molday et al., 1972) were then added to the sets of k_A and k_B values and the individual k_{int} values for each amide location were calculated at the different experimental temperatures. By this procedure, the sequence-specific corrections were assumed to be independent of the temperature and the constant for catalysis by water (k_w) was considered independent of the sequence-specific acid correction because the experimental pH* values were not extremely low (Jeng and Englander, 1991).

The equilibrium constants for local destructuring (K_l), as recovered from the experimental k_{app} values (Eq. 3), are reported in Table 1. Overall thermal unfolding of TTF-1 HD should be negligible in the range 273.4–284.0 K, i.e. below 1% (Damante et al., 1994b), which supports the assumption of an EX2 exchange regime (Hvidt and Nielsen, 1966), involving, by definition, only local opening events.

Figure 1 displays the apparent exchange rates (a) and the local destructuring equilibrium constants (b) obtained at 284.0 K. Two features are immediately evident from these plots: (i) a substantial analogy between the trends of k_{app} and K_l; these trends closely reflect the secondary structure of the molecule, although a sort of smoothing appears to reduce the excursion span in the K_l curve; and (ii) in many locations the local closed conformation does not appear strongly favoured over the open one, even in the regular helical regions. In addition to the sharply high values at the terminal region of helix III (on which we will comment in the Discussion section), the K_l constants exhibit, in general, significantly higher values than the corresponding quantities reported for the helical regions of a typical globular protein like BPTI (Wagner et al., 1984). Whilst this result is the expected consequence of a large thermal stability difference between the two proteins, the divergence appears more interesting when the effect of temperature on local fluctuations is considered. van 't Hoff plots of ln K_l versus 1/T proved almost systematically nonlinear. Since a larger number of experimental points would be necessary to demonstrate soundly the nonlinearity of van 't Hoff curves, only an analysis based on linear fit is rigorously viable, also in view of the narrow temperature range that was experimentally explored. The results are given in Table 1 and plotted in Fig. 1c as ΔH for the local destructuring equilibrium versus residue number. The observed trend shows a clear predominance of negative ΔH values along the sequence of TTF-1 HD. Since, in the experimental temperature range, local destructuring fluctuations should most likely report only short-range elementary processes, at variance with the overall unfolding transition (Hvidt and Nielsen, 1966; Englander and Kallenbach, 1984), these negative ΔH values suggest that the individual secondary structure elements of TTF-1 HD are stabilized mainly by hydrophobic interactions (Pratt and Chandler, 1977; Tanford, 1980; Wagner et al., 1984). Although experimental data are not available for the whole sequence because of detectability problems that were encountered at the lowest temperature, the helical segments of the molecule appear

in the regions which benefit most, albeit to different extents, from hydrophobic stabilization, as opposed to the loop and turn segments. Rather than lacking hydrophobic stabilization, the latter regions, however, may be regarded as fragments where hydrophobic and hydrophilic interactions nearly balance each other or even as being poorly stabilized by hydrophilic and van der Waals interactions (Wagner et al., 1984).

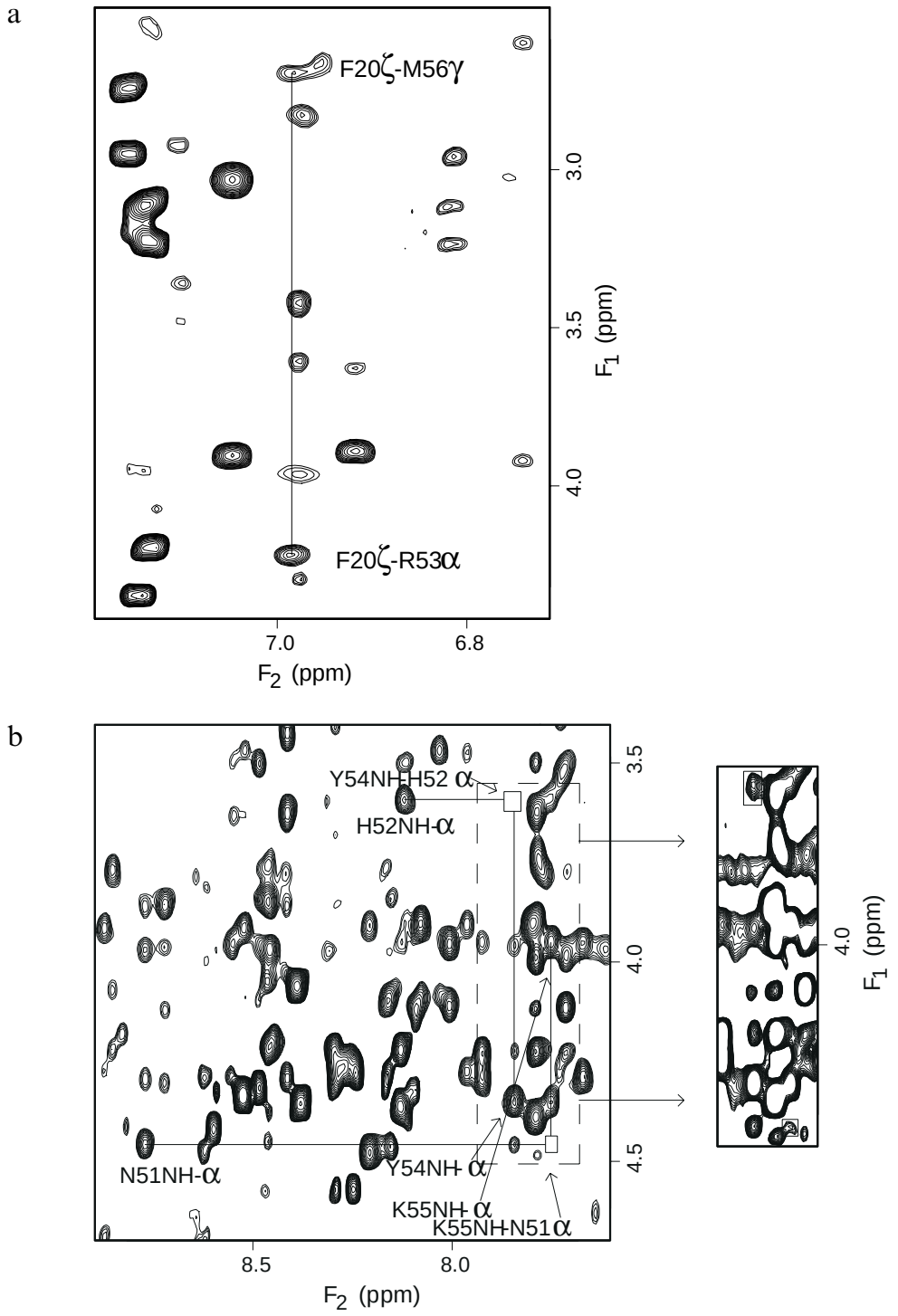

Fig. 3. Specific regions of the 2D NOESY (Jeener et al., 1979) spectrum of TTF-1 HD showing (a) the long-range contacts of Met[56] and Arg[53] to Phe[20] and (b) some relevant α_i-NH_{i+2} and α_i-NH_{i+4} connectivities at the start of the C-terminal extension of helix III. The dashed box region in (b) is shown at a higher contour level. Amino acid single-letter code is employed. The plots are taken from a 500 MHz spectrum with $t_m = 149.9$ ms. The same NOEs were also observed at lower mixing times and in NOESY spectra taken at 600 MHz ($t_m = 40$ and 60 ms) with a Bruker AMX spectrometer.

Discussion and Conclusions

Interpreting the extension of the recognition helix

According to Qian et al. (1994), the persistence of a helical structure in the C-terminal region of the recognition helix of isolated homeodomains requires a bulky hydrophobic residue at position 56, which establishes packing interactions with the molecular core. This is why sequences like *ftz* (Qian et al., 1994), *oct-3* POU (Morita et al., 1993) and NK-2 HD (Tsao et al., 1994), with Ser, Gly and Thr, respectively, at position 56, lack the C-end extension of the recognition helix. Tsao and co-workers (1994) propose that the bulky hydrophobic side-chain of residue 56 should be necessary only to balance the unfavourable solvent exposure of an additional hydrophobic amino acid at position 54. However, when residues 54 and 56 are both hydrophilic, helix III may either elongate, as in the isolated α2 HD (Phillips et al., 1991) (with Arg and Glu at 54 and 56, respectively), or break at residue 53, as in *oct-2* (Sivaraja et al., 1994) and *oct-1* POU HD (Cox et al., 1995) (both with Gln and Glu at 54 and 56, respectively).

Side-chain interactions therefore seem to play a crucial role for stability of the C-terminal segment of helix III. This peptide stretch, in fact, protrudes from the bulk of the three-helix motif into the solvent only in isolated homeodomains. In the HD-DNA complex, it contributes to the recognition and binding by entering into the major groove, even when it is poorly structured in the isolated homeodomain, as is observed with *oct-1* POU (Klemm et al., 1994; Cox et al., 1995) and NK-2 HD (Tsao et al., 1994).

For TTF-1 HD, where bulky hydrophobic residues occur at both positions 54 and 56, the average number of connectivities per residue in the fragment 51–59 is smaller than that of other structured regions of the molecule (Esposito et al., 1996), and the difference is mostly due to the lack of interresidue side-chain NOEs. The observed interresidue NOE contacts for the fragment 51–59 include only connectivities of backbone and β-hydrogens, in addition to the long-range contacts of Arg^{53} and Met^{56} to Phe^{20}. A summary diagram of the main-chain NOEs and other relevant NMR evidence, observed for the recognition helix of TTF-1 HD, is given in Fig. 2. Besides the NOEs reported in this figure and the long-range ones of Fig. 3a, two additional contacts are worth mentioning, namely Asn^{51}αH–Lys^{55}NH and His^{52}αH–Tyr^{54}NH (Fig. 3b), which are both extremely weak and consistent with an α-helix as are those of Fig. 2. Only rarely, however, did we observe the α_i-NH_{i+2} connectivity type in α-helical regions of TTF-1 HD, and the detection of such contact in a supposedly not very rigid fragment of the molecule was rather surprising. The separation α_i-NH_{i+2} is larger than α_i-NH_{i+4} in regular α-helices and becomes sensibly smaller only in 3_{10}-helices, where, conversely, the α_i-NH_{i+4} distance is too long (>5 Å; 1 Å = 0.1 nm) for the corresponding connectivity to be detected in NOESY spectra under ordinary conditions (Wüthrich, 1986).

These observations, along with evidence obtained from the initial isotope exchange determinations (Fig. 2), suggested that some small-amplitude local motion should take place in correspondence of residues 51, 52 and 53, which may either kink the C-terminal extension with

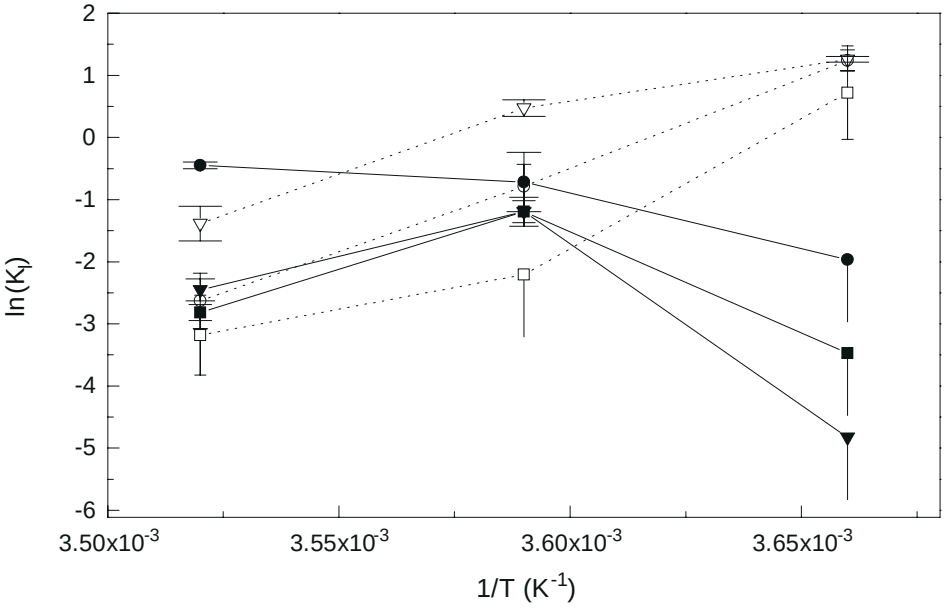

Fig. 4. van 't Hoff plot for local opening equilibrium in the C-terminal extension and other representative positions of the recognition helix of TTF-1 HD. Solid lines and symbols refer to Asn^{51} (circles), His^{52} (triangles) and Arg^{53} (squares). Dashed lines and empty symbols refer to Ile^{47} (squares), Gln^{50} (circles) and Arg^{58} (triangles). Uncapped, single-sided error bars are drawn when K_I is obtained from the corresponding upper-limit value of k_{app} (see text and Table 1).

respect to the preceding portion of helix III or slightly elongate the whole helix III by tightening of the local geometry into a 3_{10}-helix. A knowledge of the local destructuring equilibrium constants (K_l) may provide clues to the actual structure dynamics, and an inspection of Table 1 shows a very interesting trend along the whole of helix III. The K_l values, in fact, decrease with increasing temperature up to Gln[50]. At Asn[51] this trend is totally reversed, whilst at His[52] and Arg[53] the reversal is only partial. At Arg[58] the original behaviour is eventually restored (Fig. 4). These results indicate that fluctuations leading to local structure opening are preferentially balanced by hydrophobic interactions along the whole helix III, *including the C-terminal extension*, except for Asn[51] where hydrophobic interactions appear to have been nearly overcome at the temperature conditions of the NOESY spectra. By further temperature increase, the dominant process is no longer the local opening equilibrium but rather a concerted opening, as suggested by the H-D exchange results at 287 K (Viglino et al., 1993). Below 278 K, however, hydrophobic interactions become less effective over the entire fragment 51–53. The relevance of hydrophobic interactions in stabilizing TTF-1 HD structure has already been pointed out when discussing H-D exchange data (Fig. 1c). Since in isolated TTF-1 HD and any isolated HD, the C-terminal extension of helix III leans out of the molecular core into the solvent, a residual stabilization must be operative, at least up to Arg[58], if the typical helix connectivities are preserved and the backbone amide of the latter residue is exchange-protected. In addition to the packing with the structure core mediated by residue 56 (Fig. 3a), further stabilization should also arise from local transient interactions among the bulky side-chains of the fragment 54–59. Favourable packing interactions with the molecular core should be much more direct for residues 51, 52 and 53, but the behaviour of Asn[51], in spite of its closeness to the core, suggests that this invariant residue, together with the nearly invariant Arg[53] (occurrence >99%) (Gehring et al., 1994a) and with His[52], must represent a group of strictly conserved conformation determinants, probably the remnant of a common ancestor evolved from prokaryotic HTH motifs. A statistical survey on protein helices confirms that these three types of residues prevalently occur at helix termini (Richardson and Richardson, 1988), but while His and Arg exhibit large frequencies (>3 standard deviations) at C-ends, Asn occurs most commonly at the N-cap position. The consequences induced by Asn[51] are a loosening of the helix and an associated break of stabilizing cooperativity of the H-bond network. The side-chain hydrophobic interactions of the subsequent dipeptide should partially suppress these effects and assist a gradual restoration of the helix order. In TTF-1 HD this recovery is parallel to the progressive decrease of the K_l constants along the tripeptide segment 51–53. At the extremely conserved Arg[53] a firmer link to the previous helix, assisted by the contact to the Phe[20] ring (Fig. 3a), can be restored most likely via an H-bond of the same Arg[53] backbone amide to Gln[50]CO, as judged from the i-i+2 interaction between His[52] and Tyr[54].

TABLE 2
SECONDARY STRUCTURE ADOPTED IN NON-HOMEODOMAIN SEQUENCES BY THE MOST COMMON FRAGMENTS 51–53 OF HOMEODOMAIN MOTIFS[a]

Sequence[b]	α-Helix[c]	α-Helix initiation/termination[d]	Others[e]
AsnHisArg[f]	0	3	2
AsnLysArg[g]	3	6	2
AsnArgArg[h]	5	3[i]	6

[a] Secondary structure classification according to Kabsch and Sander (1983).
[b] The structures where the listed sequences occur are named by using the Brookhaven Protein Databank code.
[c] Only when the α-helix extends over the four preceding and the four subsequent residues.
[d] Only when the α-helix breaks or starts in the fragment or within the subsequent four residues. A termination/initiation entails transition from/to α-helix to/from any other geometry, including 3_{10}-helix.
[e] H-bonded turns, bends, extended and unclassified secondary structure.
[f] Occurring in: 1EFG, 1TAD, 2BOP, 4RHV, 8ACN.
[g] Occurring in: 1BMT, 1CPC, 1DHR, 1DHX, 1GKY, 1HAR, 1HPM, 1HYM, 1MIN, 2HPD, 1TCT.
[h] Occurring in: 1AAK, 1AOZ, 1APL, 1FBA, 1GTR, 1HRT, 1LIS, 1MYP, 1TPK, 1WHT, 2BBV, 2STV, 2TBV, 3GLY.
[i] Including a transition from turn into 3_{10}-helix.

The loss of H-bond cooperativity at Asn[51], coupled to the small-amplitude fluctuations within the stretch 51–53 and to local shift of the helix H-bond register at Arg[53], is responsible for the displacement of the subsequent helix NH vector directions from their optimal positions for H-bond formation and, as a consequence, for the observed fast exchange of the backbone amides of the segment 54–57. The slow-exchange response of Arg[58]NH confirms this pattern because the first carbonyl capable of establishing an H-bond with it (Tyr[54]CO) lies outside the stretch 51–53.

Irrespective of the geometry adopted at the fragment 51–53 and of the persistence of a helical folding at the C-terminal region of helix III in isolated homeodomains, relating the nearly absolute invariance of Asn[51] and Arg[53] to the conformational effects they should be able to impart suggests that a conformation-determinant fragment is universally present in an HD recognition helix.

This interpretation can be tested further by an examination of the protein structure database. A search over a representative collection (1322 sequences), compiled according to structure uniqueness criteria (Hobohm and Sander, 1995), shows that the tripeptides AsnHisArg, AsnLysArg and AsnArgArg, which respectively account for 3.6, 5.7 and 87.8% of occurrences at locations 51-52-53 of HD sequences (Gehring et al., 1994a), are shared by

30 structures other than HD motifs (Table 2). Apart from 10 sequences where the fragments are found in H-bonded turns, bends, extended or even unclassified secondary structure elements (Kabsch and Sander, 1983), in the remaining 20 structures the three stretches are either involved in α-helices (eight structures) or in their initiation/termination via transition into 3_{10}-helix or turn geometry (12 structures). The observation of helix initiation/termination is more frequent with AsnHisArg and AsnLysArg, but a significant occurrence of the feature can be appreciated also for AsnArgArg (Table 2), i.e. the HD consensus residues for positions 51, 52 and 53.

Functional implications and concluding remarks

The tertiary structure of TTF-1 HD matches the general folding pattern of isolated homeodomains (Esposito et al., 1996). Yet the DNA-binding specificity of TTF-1 HD (like for all other members of the NK-2 subfamily) is unusual (Guazzi et al., 1990).

Perhaps the most interesting results of the present investigation come from the attempt to delineate the conformational dynamics of the C-terminal extension of helix III, i.e. the recognition helix which engages most of the interactions with the major groove of the DNA operator (Gehring, 1987; Pabo and Sauer, 1992; Gehring et al., 1994b).

We suggest that in TTF-1 HD, helix III undergoes a local fluctuation of the tripeptide 51–53 which breaks the continuity with the flanking helical segments. Similar breaks of helix III continuity have also been described for *Antp* (Billeter et al., 1990), LFB1/HNF1 (Leiting et al., 1993) and α2 HD (Phillips et al., 1991), whilst for *ftz* (Qian et al., 1994), NK-2 (Tsao et al., 1994), *oct-3* POU (Morita et al., 1993), *oct-2* POU (Sivaraja et al., 1994) and *oct-1* POU HD (Cox et al., 1995) the helical order appeared spoiled next to residue 50 because of poor packing with the molecular core.

Independent of the adopted arrangement, a general conclusion, which may hold true for all homeodomains, is the presence of a conformation determinant at the fragment 51–53 of the recognition helix. The occurrence of such an arrangement might be related to the fine-tuning of the recognition process and/or to fundamentally distinct prokaryotic (i.e. repressor-like) and eukaryotic (i.e. homeodomain-like) DNA-binding modes (Xu et al., 1995; Damante et al., 1996).

On the other hand, the structural data available on canonical HD-DNA complexes (Kissinger et al., 1990; Wolberger et al., 1991; Billeter et al., 1993; Klemm et al., 1994; Tsao et al., 1994) invariably show that a single elongated helix III docks into the major groove. Thus, a possible functional role for the conformational mobility of the recognition helix as observed in isolated homeodomains should be addressed.

Evidence that multiple conformational options of proteins are relevant to their DNA binding comes from the recent thermodynamic study of Spolar and Record (1994). Extensive scrutiny of the available data demonstrates that site-specific protein-DNA recognition entails a large negative heat capacity change (ΔC_p). Analysis of these ΔC_p values and of ΔS values for protein-DNA complexation indicates that binding is coupled to local conformational changes, most prevalent on the protein which undergoes a sort of induced-fit transition. The protein's negative ΔC_p is then the thermodynamic signature of the induced-fit mechanism which arises mainly by changes in the exposure to water of the nonpolar protein surface (Spolar and Record, 1994).

Since preliminary results suggest that TTF-1 HD, like the highly homologous NK-2 HD (Tsao et al., 1994), undergoes a substantial stabilization upon DNA binding, the NMR evidence presented in Fig. 1c shows that this homeodomain meets the requirements involved by the induced-fit model. The stabilization of most of the structural elements of the molecule, and in particular of the recognition helix (Figs. 1c and 4), is hydrophobic in nature and, without any doubt, DNA binding reduces the solvent-accessible surface area. Our H-D exchange determinations do not enable a rigorous conclusion to be drawn about the possible presence of negative ΔC_p values for local conformational stabilization because only three temperature data sets were available. Therefore, the nonlinearity of van 't Hoff plots was ignored when determining the ΔH values for local destructuring equilibria. Nevertheless, negative ΔH values, suggesting local hydrophobic stabilization, were obtained for most of the residues in TTF-1 HD (Fig. 1c), which could then be considered as necessary (but not sufficient) conditions required by an induced-fit process upon DNA binding. In assessing the conformational stability of the extension of helix III, however, we superseded the previous interpretation policy due to the local trend of the systematic deviations from linearity (Fig. 4). It is tempting to notice that the resulting picture adheres very well to the induced-fit model in a region where crucial conformational changes are expected upon complexation (e.g. local helix rearrangement and shift in the rotamer distribution of Tyr^{54}) (Fogolari et al., 1993; Esposito et al., 1996). If an analogous *released* criterion were applied extensively, the data of Table 1 would definitely demonstrate the possibility of negative ΔC_p for the conformational stabilization of TTF-1 HD. Direct isotope exchange measurements on the TTF-1 HD-DNA complex will anyway be necessary to confirm the induced-fit model, i.e. to determine whether burial of hydrophobic surfaces balances the unfavourable contributions to the binding entropy, mostly due to the loss of local conformational freedom on association-coupled adjustments of the homeodomain structure (Sivaraja et al., 1994; Spolar and Record, 1994).

Acknowledgements

The authors wish to thank CNR and AIRC for financial support. The suggestions of Dr. A. Makek and the courtesy of Prof. G. Bodenhausen, for access to the 600 MHz spectrometer of the Suisse Romande High Field NMR Facility, are also acknowledged.

References

Bax, A., Ikura, M., Kay, L.E. and Zhu, G. (1991) *J. Magn. Reson.*, **91**, 174–178.

Bell, J.A., Becktel, W.J., Sauer, U., Baase, W.A. and Matthews, B.W. (1992) *Biochemistry*, **31**, 3590–3596.

Billeter, M., Qian, Y.Q., Otting, G., Müller, M., Gehring, W.J. and Wüthrich, K. (1990) *J. Mol. Biol.*, **214**, 183–197.

Billeter, M., Qian, Y.Q., Otting, G., Müller, M., Gehring, W.J. and Wüthrich, K. (1993) *J. Mol. Biol.*, **234**, 1084–1097.

Bohinski, R.J., Di Lauro, R. and Whitsett, J.A. (1994) *Mol. Cell. Biol.*, **14**, 5671–5681.

Ceska, T.A., Lamers, M., Monaci, P., Nicosia, A., Cortese, R. and Suck, D. (1993) *EMBO J.*, **12**, 1805–1810.

Clarke, N.D. (1995) *Protein Sci.*, **4**, 2269–2278.

Covington, A.K., Robinson, R.A. and Bates, R.G. (1966) *J. Phys. Chem.*, **70**, 3820–3824.

Cox, M., Van Tilborg, P.J.A., De Laat, W., Boelens, R., Van Leeuwen, H.C., Van der Vliet, P.C. and Kaptein, R. (1995) *J. Biomol. NMR*, **6**, 23–32.

Damante, G. and Di Lauro, R. (1991) *Proc. Natl. Acad. Sci. USA*, **88**, 5388–5392.

Damante, G., Fabbro, D., Pellizzari, L., Civitareale, D., Guazzi, S., Polycarpou-Schwartz, M., Cauci, S., Quadrifoglio, F., Formisano, S. and Di Lauro, R. (1994a) *Nucleic Acids Res.*, **22**, 3075–3083.

Damante, G., Tell, G., Leonardi, A., Fogolari, F., Bortolotti, N., Di Lauro, R. and Formisano, S. (1994b) *FEBS Lett.*, **354**, 293–296.

Damante, G., Pellizzari, L., Esposito, G., Fogolari, F., Viglino, P., Fabbro, D., Tell, G., Formisano, S. and Di Lauro, R. (1996) *EMBO J.*, **15**, 4992–5000.

Englander, S.W. and Kallenbach, N.R. (1984) *Q. Rev. Biophys.*, **16**, 521–655.

Esposito, G., Fogolari, F., Damante, G., Formisano, S., Tell, G., Leonardi, A., Di Lauro, R. and Viglino, P. (1996) *Eur. J. Biochem.*, **241**, 101–113.

Fogolari, F., Esposito, G., Viglino, P., Damante, G. and Pastore, A. (1993) *Protein Eng.*, **6**, 513–519.

Gehring, W.J. (1987) *Science*, **236**, 1245–1252.

Gehring, W.J., Affolter, M. and Bürglin, T. (1994a) *Annu. Rev. Biochem.*, **63**, 487–526.

Gehring, W.J., Qian, Y.Q., Billeter, M., Furukubo-Tokunaga, K., Schier, A.F., Resendez-Perez, D., Affolter, M., Otting, G. and Wüthrich, K. (1994b) *Cell*, **78**, 211–223.

Griesinger, C., Otting, G., Wüthrich, K. and Ernst, R.R. (1988) *J. Am. Chem. Soc.*, **110**, 7870–7872.

Guazzi, S., Price, M., De Felice, M., Damante, G., Mattei, M.-G. and Di Lauro, R. (1990) *EMBO J.*, **9**, 3631–3639.

Hobohm, U. and Sander, C. (1995) *J. Mol. Biol.*, **251**, 390–399.

Hvidt, A. and Nielsen, S.O. (1966) *Adv. Protein Chem.*, **21**, 287–386.

Jeener, J., Meier, B.H., Bachmann, P. and Ernst, R.R. (1979) *J. Chem. Phys.*, **71**, 4546–4553.

Jeng, M.-F. and Englander, S.W. (1991) *J. Mol. Biol.*, **221**, 1045–1061.

Kabsch, W. and Sander, C. (1983) *Biopolymers*, **22**, 2577–2637.

Kissinger, C.R., Liu, B., Martin-Blanco, E., Kornberg, T.B. and Pabo, C.O. (1990) *Cell*, **63**, 579–590.

Klemm, J.D., Rould, M.A., Aurora, R., Herr, W. and Pabo, C.O. (1994) *Cell*, **77**, 21–32.

Leiting, B., De Francesco, R., Tomei, L., Cortese, R., Otting, G. and Wüthrich, K. (1993) *EMBO J.*, **12**, 1797–1803.

Marion, D. and Wüthrich, K. (1983) *Biochem. Biophys. Res. Commun.*, **113**, 967–974.

Marion, D. and Bax, A. (1989) *J. Magn. Reson.*, **83**, 205–211.

Molday, R.S., Englander, S.W. and Kallen, R.G. (1972) *Biochemistry*, **11**, 150–158.

Morita, E.H., Shirakawa, M., Hayashi, F., Imagawa, M. and Kyogoku, Y. (1993) *FEBS Lett.*, **321**, 107–110.

Otting, G., Qian, Y.Q., Billeter, M., Müller, M., Affolter, M., Gehring, W.J. and Wüthrich, K. (1988) *EMBO J.*, **7**, 4305–4309.

Otting, G., Qian, Y.Q., Billeter, M., Müller, M., Affolter, M., Gehring, W.J. and Wüthrich, K. (1990) *EMBO J.*, **9**, 3085–3092.

Pabo, C.O. and Sauer, R.T. (1992) *Annu. Rev. Biochem.*, **61**, 1053–1095.

Phillips, C.L., Vershon, A.K., Johnson, A.D. and Dahlquist, F.W. (1991) *Genes Dev.*, **5**, 764–772.

Pratt, L.R. and Chandler, D. (1977) *J. Chem. Phys.*, **67**, 3683–3704.

Presta, L.G. and Rose, G.D. (1988) *Science*, **240**, 1632–1641.

Qian, Y.Q., Billeter, M., Otting, G., Müller, M., Gehring, W.J. and Wüthrich, K. (1989) *Cell*, **59**, 573–580.

Qian, Y.Q., Otting, G., Billeter, M., Müller, M., Gehring, W.J. and Wüthrich, K. (1993) *J. Mol. Biol.*, **234**, 1070–1083.

Qian, Y.Q., Furukubo-Tokunaga, K., Resendez-Perez, D., Müller, M., Gehring, W.J. and Wüthrich, K. (1994) *J. Mol. Biol.*, **238**, 333–345.

Richardson, J.S. (1981) *Adv. Protein Chem.*, **34**, 167–339.

Richardson, J.S. and Richardson, D.C. (1988) *Science*, **240**, 1648–1652.

Sivaraja, M., Botfield, M.C., Mueller, M., Jancso, A. and Weiss, M.A. (1994) *Biochemistry*, **33**, 9845–9855.

Spolar, R.S. and Record Jr., M.T. (1994) *Science*, **263**, 777–784.

Tanford, C. (1980) *The Hydrophobic Effect: Formation of Micelles and Biological Membranes*, Wiley, New York, NY, U.S.A.

Tsao, D.H.H., Gruschus, J.M., Wang, L.-H., Nirenberg, M. and Ferretti, J.A. (1994) *Biochemistry*, **33**, 15053–15060.

Viglino, P., Fogolari, F., Formisano, S., Bortolotti, N., Damante, G., Di Lauro, R. and Esposito, G. (1993) *FEBS Lett.*, **336**, 397–402.

Wagner, G. and Wüthrich, K. (1982) *J. Mol. Biol.*, **160**, 343–361.

Wagner, G., Stassinopoulou, C.I. and Wüthrich, K. (1984) *Eur. J. Biochem.*, **145**, 431–436.

Wolberger, C., Vershon, A.K., Liu, B., Johnson, A.D. and Pabo, C.O. (1991) *Cell*, **67**, 517–528.

Wüthrich, K. (1986) *NMR of Proteins and Nucleic Acids*, Wiley, New York, NY, U.S.A.

Xu, W., Rould, M.A., Jun, S., Desplan, C. and Pabo, C.O. (1995) *Cell*, **80**, 639–650.

Zhou, H.X., Pinker, R.J. and Kallenbach, N.R. (1993) *Biochemistry*, **32**, 421–425.